Effects of Pressure on the Fundamental Physics of Fuel Injection in Diesel Engines

J. C. Oefelein*, R. N. Dahms, G. Lacaze, J. L. Manin, L. M. Pickett
Combustion Research Facility, Sandia National Laboratories, Livermore CA, USA
oefelei@sandia.gov, rndahms@sandia.gov, gnlacaz@sandia.gov, jmanin@sandia.gov, lmpicke@sandia.gov

Abstract

This paper provides an analysis of high-pressure phenomena and its potential effects on the fundamental physics of fuel injection in Diesel engines. We focus on conditions when cylinder pressures exceed the thermodynamic critical pressure of the injected fuel and describe the major differences that occur in the jet dynamics compared to that described by classical spray theory. To facilitate the analysis, we present a detailed model framework based on the Large Eddy Simulation (LES) technique that is designed to account for key high-pressure phenomena. Using this framework, we perform a detailed analysis using the experimental data posted as part of the Engine Combustion Network (see www.sandia.gov/ECN): namely the "Baseline n-heptane" and "Spray-A (n-dodecane)" cases, which are designed to emulate conditions typically observed in Diesel engines. Calculations are performed by rigorously treating the experimental geometry, operating conditions and relevant thermo-physical gas-liquid mixture properties. Results are further processed using linear gradient theory, which facilitates calculations of detailed vapor-liquid interfacial structures, and compared with the high-speed imaging data. Analysis of the data reveals that fuel enters the chamber as a compressed liquid and is heated at supercritical pressure. Further analysis suggests that, at certain conditions studied here, the classical view of spray atomization as an appropriate model is questionable. Instead, nonideal real-fluid behavior must be taken into account using a multicomponent formulation that applies to arbitrary hydrocarbon mixtures at high-pressure supercritical conditions.

Introduction

Research over the past decade has provided significant insights into the structure and dynamics of multiphase flows at high pressures [1–12]. Most of this research has been done in the context of liquid-rocket propulsion, which involves direct injection of both liquid fuel and oxidizer into the combustion chamber. However, the observed trends are equally valid for other liquid fueled devices. Here we focus on Diesel engines at conditions where the fuel is injected at conditions that exceed the thermodynamic critical pressure.

Injection of liquid fuel in systems where the working fluid exceeds the thermodynamic critical pressure of the liquid phase is not well understood. Depending on pressure, injected jets can exhibit two distinctly different sets of evolutionary processes. At low subcritical pressures, the classical situation exists where a well-defined molecular interface separates the injected liquid from ambient gases due to the presence of surface tension. Interactions between dynamic shear forces and surface tension promote primary atomization and secondary breakup processes that evolve from a dense state, where the liquid exists as sheets filaments or lattices intermixed with sparse pockets of gas; to a dilute state, where drop-drop interactions are negligible and dilute spray theory can be used. As ambient pressures approach or exceed the critical pressure of the liquid, however, the situation may become quite different. Under these conditions, interfacial diffusion layers can develop as a consequence of both vanishing surface tension forces and locally diminishing gas-liquid interfaces. The lack of inter-molecular forces and a distinct interfacial structure promotes diffusion dominated mixing processes prior to atomization. As a consequence, injected jets evolve in the presence of exceedingly large but continuous thermo-physical gradients in a manner that is markedly different from the classical assumptions.

Modeling either of the two extremes described above poses a variety of challenges. To enhance our understanding of these processes in the context of Diesel engines, we have performed a series of calculations using the Large Eddy Simulation (LES) technique and combined this with 1) key experimental observations, and 2) the development of a detailed theoretical framework to explain the observed trends. We use the experimental data provided by Pickett *et al*. as part of the Engine Combustion Network (see www.ca.sandia.gov/ECN [13]) using the "Baseline n-heptane" and "Spray-A (n-dodecane)" cases as key targets. Significant attention is focused on corroborating measured and modeled results as a function of distinctly different phenomenological processes that occur as a function of pressure. This is accomplished by rigorously treating the experimental geometry (injector and vessel) and operating conditions with a fully integrated state-of-the-art model framework.

*Corresponding author: oefelei@sandia.gov

Approach

Experimental imaging of injection processes at supercritical pressures suggests that drop breakup processes occur at low ambient temperatures but diffusion dominated mixing occurs without apparent formation of fuel drops at engine-relevant high ambient temperature conditions. To explain this transition, we first apply LES to understand the state of the local mixture. We then extend our real-fluid model framework to account for multicomponent vapor-liquid equilibrium, the presence of surface tension, and the resultant interface states. Using this framework, linear gradient theory is then applied to reconstruct the detailed interface structure at these conditions.

LES is performed using a single unified code framework called "RAPTOR." The baseline theoretical formulation and related subgrid-scale (SGS) models are described by Oefelein [14]. Unlike conventional solvers, RAPTOR is a Direct Numerical Simulation (DNS) solver that has been optimized to meet the strict algorithmic requirements imposed by the LES formalism. The theoretical framework solves the fully coupled conservation equations of mass, momentum, total-energy and species for a chemically reacting flow using multicomponent or mixture-averaged formulations. It is designed to handle high-Reynolds-number, high-pressure, real-gas and/or liquid conditions over a wide Mach operating range. It accounts for detailed thermodynamic and transport processes and is sophisticated in its ability to handle a generalized SGS model framework. The code is capable of treating multiphase flows using either a Lagrangian-Eulerian formulation or pure-Eulerian real-fluid model. A noteworthy aspect of RAPTOR is that it is designed specifically for LES using non-dissipative, discretely-conservative differencing stencils. This eliminates numerical contamination of the SGS models and provides discrete conservation properties that are imperative for LES. Representative case studies are given by Oefelein *et al.* [6, 15–20].

The real-fluid property evaluation scheme employed in RAPTOR is designed to account for thermodynamic nonidealities and transport anomalies over a wide range of pressures and temperatures. The scheme is comprehensive and intricate, thus only a skeletal description can be given here. The extended corresponding states model [21, 22] is employed using either Benedict-Webb-Rubin (BWR) or cubic equations of state to evaluate the *p-v-T* behavior of the inherent dense multicomponent mixtures. Use of modified BWR equations of state in conjunction with the extended corresponding states principle has been shown to provide consistently accurate results over the widest range of pressures, temperatures and mixture states, especially at near-critical conditions. A major disadvantage of the BWR equations, however, is that they are not computationally efficient. Cubic equations of state can be less accurate, especially for mixtures at near-critical or saturated conditions, but are computationally efficient. Experience has shown that both the Soave-Redlich-Kwong (SRK) and Peng-Robinson (PR) equations, when used in conjunction with the corresponding states principle, can give accurate results over the range of pressures, temperatures and mixture states typically of interest. SRK coefficients are fit to vapor pressure data and thus more suitable for conditions when reduced temperatures are less than one. PR coefficients, on the other hand, are more suitable for conditions when reduced temperatures are greater than one. A summary of the cubic equations of state and recommended constants is given by Reid *et al.* [23, Chapter 3].

Having established an analytical representation for real mixture *p-v-T* behavior, thermodynamic properties are obtained in two steps. First, respective component properties are combined at a fixed temperature using the extended corresponding states methodology outlined above to obtain the mixture state at a given reference pressure. A pressure correction is then applied using departure functions of the form given by Reid *et al.* [23, Chapter 5]. These functions are exact relations derived using Maxwell's relations (see for example VanWylen and Sonntag [24, Chapter 10]) and make full use of the real mixture *p-v-T* path dependencies dictated by the selected equation of state. Standard state properties are obtained using the databases developed by Gordon and McBride [25] and Kee *et al.* [26]. Chemical potentials and fugacity coefficients are obtained in a similar manner. Likewise, viscosity and thermal conductivity are obtained using the extended corresponding states methodologies developed by Ely and Hanley [27, 28]. Mass and thermal diffusion coefficients are obtained using the methodologies outlined by Bird *et al.* [29] and Hirschfelder *et al.* [30] in conjunction with the corresponding states methodology of Takahashi [31].

To augment the analysis presented below, the real-fluid framework described above is combined with Vapor-Liquid Equilibrium (VLE) and Linear Gradient (LG) theory to facilitate the calculation of the detailed vapor-liquid interfacial structure for the multicompnent mixtures of interest. LG theory provides a thermo-mechanical model of continuous fluid media. At equilibrium, as applied in this paper, the model has been shown in detail to be equivalent to mean-field molecular theories of capillarity. The foundations of this theory were established by van der Waals in 1894 and reformulated later by Cahn and Hilliard [32]. In the last decades, gradient theory has been successfully applied to a wide variety of fluids including vapor-liquid and liquid-liquid interfaces associated with hydrocarbon mixtures, polar compounds and polymers. Recently, the LG model has been successfully compared to Monte Carlo molecular simulations of vapor-liquid and liquid-liquid interfaces aimed at capturing both surface tension and the details of the corresponding molecular interfacial structures [33–35]. Using LG theory, both surface tension and the interface thickness can be calculated through integration along the interfacial density profile.

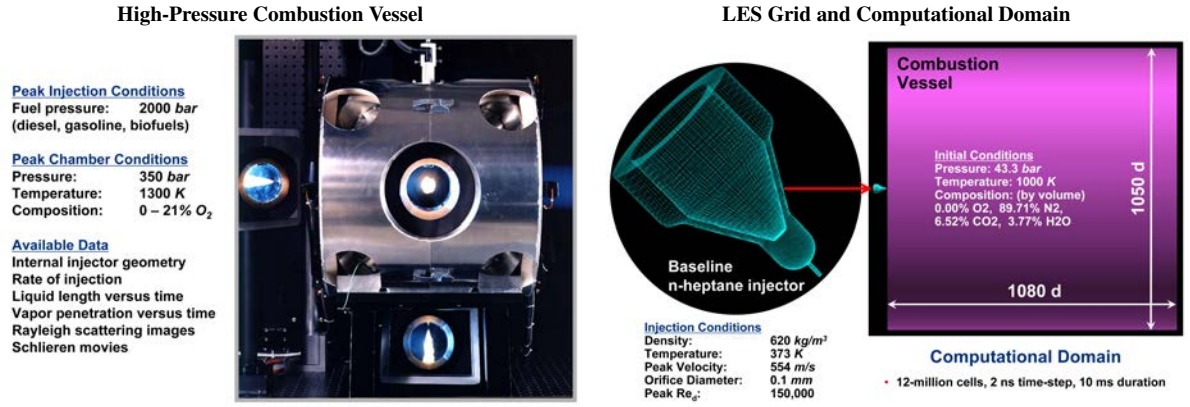

Figure 1: Photograph of the Sandia high-pressure combustion vessel (left) and computational domain used for LES (right). The injector is mounted at the head-end of the vessel, as indicated by the red arrow. The grid and operating conditions identically match the experiment. Conditions listed correspond to the Baseline n-Heptane experiment.

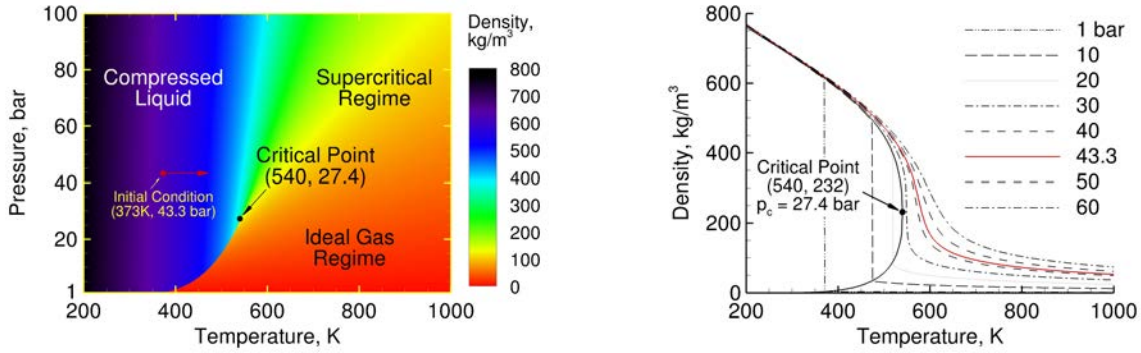

Figure 2: Thermodynamic characteristics of n-heptane showing key regimes and its initial state when injected into the combustion vessel. The jet enters as a compressed liquid and is heated at supercritical pressure.

Results and Discussion

Using a combination of LES, the real-fluid model, VLE and LG theory, we have performed an integrated series of studies aimed at understanding the effects of pressure on interfacial injection dynamics. To facilitate the analysis, we considered the operating conditions associated with two key experiments being studied by Pickett *et al*. [13]: namely the "Baseline n-heptane" and "Spray-A (n-dodecane)" cases. These experiments are designed to emulate conditions typically observed in a Diesel engine. Calculations were performed by identically matching the experimental operating conditions, injector geometry, and combustion chamber.

The experimental apparatus, corresponding computational domain, and key operating conditions for the Baseline n-Heptane case are shown in Fig. 1. The experiment involves a liquid n-heptane jet injected into a hot quiescent mixture of gaseous products. For the case considered here, all the oxygen has been consumed to prevent the onset of combustion so we can focus on thermo-physical processes associated with injection. Fuel is injected with an electronically controlled common rail injector at a pressure of $1540\ bar$ and $373\ K$. The ambient gas composition in the vessel is conditioned to provide an inert composition of N_2, CO_2, and H_2O. The actual mole fractions of these components are summarized in Fig. 1. The thermodynamic characteristics of n-heptane are shown in Fig. 2. Its critical point is $540\ K$, $27.4\ bar$. Thus, n-heptane is injected into the chamber as a compressed liquid (i.e., supercritical with respect to pressure, subcritical with respect to temperature). LES calculations were performed using a grid with approximately 12-million cells. The transient jet pulse is simulated to closely approximate the actual experimental conditions. This produces a peak bulk velocity of $554\ m/s$ and corresponding jet Reynolds number of $150,000$ inside the injector nozzle. The quasi-steady portion of the pulse lasted for $6.66\ ms$. At $6.69\ ms$ the jet ramps down to zero velocity, with the end of injection occurring at $6.93\ ms$. The total integration time is $10\ ms$ using a time-step of $2\ ns$.

Figure 3 provides a representative comparison of the mixture fraction distribution predicted using LES with the corresponding experimentally measured Rayleigh images. Note that the color maps and contour spacing used

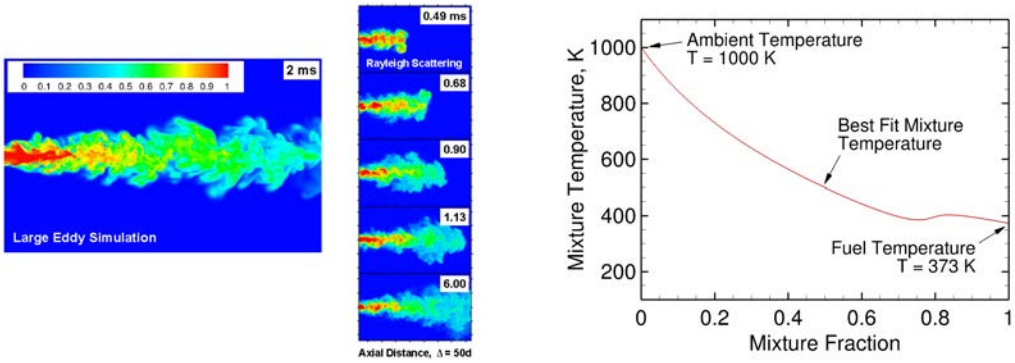

Figure 3: Comparison of mixture fraction predictions from LES (left) with measured Rayleigh images (center). Corresponding best fit mapping of temperature as a function of mixture fraction for the time evolving field (right).

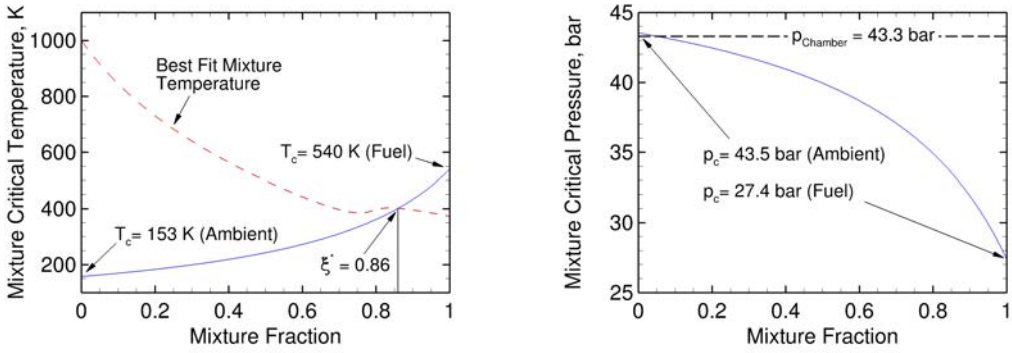

Figure 4: Mixture critical temperature and pressure of the time evolving field as a function of mixture fraction.

are identical for both the LES and measured data. In general, predictions agree well with the available experimental data. To perform a comprehensive analysis of the fuel mixing states, we used the time evolving fields given by the LES to map the relationship between mixture fraction (denoted as ξ) and temperature. Here, $\xi = 1$ represents the fuel stream (C_7H_{16}) and $\xi = 0$ represents the "oxidizer" stream (N_2-CO_2-H_2O). A scatter plot of mixture temperature conditioned on mixture fraction was produced, which revealed that there are only slight variations in mixture temperature as a function of mixture fraction. Figure 3 also shows the resultant best fit relationship.

Having established the mapping between temperature and mixture fraction, we can now analyze how the state of the local mixture varies across key thermodynamic regimes. To accomplish this, we use the fundamental assumptions built into the real fluid model to calculate the mixture critical temperature and pressure as a function of mixture fraction. We then superimpose the best fit mixture temperature shown in Fig. 3 and the nominal ambient pressure chamber condition of $43.3\ bar$ to identify key points of intersection. Figure 4 shows the results. Analysis of these data reveals two important features. First, the local mixture temperature is greater than the critical mixture temperature for all values of mixture fraction less than 0.86. Second, the nominal ambient chamber pressure is greater than the critical mixture pressure for all values of mixture fraction greater than 0.05.

Using the information given in Figs 3 and 4, we have plotted the entire envelope of mixture states on a thermodynamic regime diagram. Results are shown in Fig 5. Trends demonstrate that the mixing path associated with all states throughout the duration of injection never crosses the liquid/vapor regime (i.e., the mixture is never saturated). Instead, n-heptane is injected as a compressed liquid and the resultant local interfacial mixing layer dynamics occur at conditions that are locally supercritical. Surface tension effects are typically assumed to be negligible under such conditions, which implies that classical first order vapor-liquid phase transitions (as are typically assumed) do not occur. Instead, processes dominated by surface tension such as primary atomization, secondary breakup, and the presence of distinct drops become negligible [36, 37].

To further investigate the nature of the phase transitions at high-pressures, we extended our analysis by combining the VLE and LG models described above. Concurrently, we performed a series of imaging experiments to obtain visual evidence regarding the nature of the multiphase flow dynamics. In addition, we shifted our attention to the Spray-A cases using n-dodecane since this fuel has properties that are closer to that of an actual Diesel

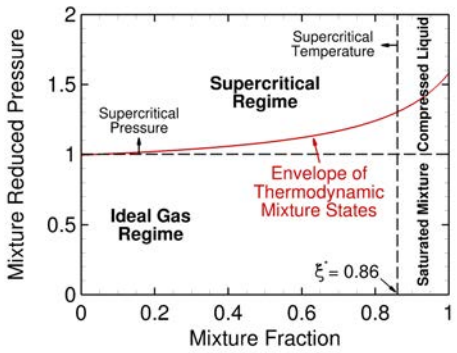

Figure 5: Envelope of mixture states predicted as a function of mixture fraction.

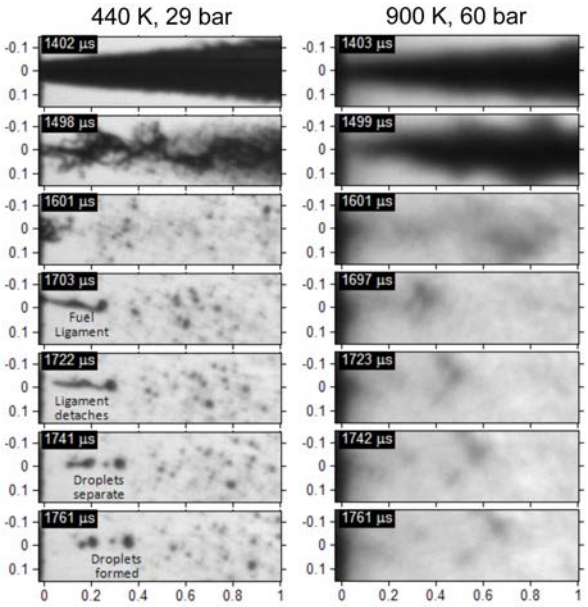

Figure 6: Visualization of liquid n-dodecane jets injected at reference conditions where the ambient gas is $p_1 = 29\ bar, T_1 = 440\ K$ and $p_2 = 60\ bar, T_2 = 900\ K$. At low temperatures there is evidence of drops and ligaments. At high temperatures there is no evidence of drops or ligaments.

engine. The critical pressure and temperature of n-dodecane are $p_c = 18.2\ bar$ and $T_c = 658\ K$, respectively. The experiments were aimed at imaging the structure of n-dodecane jets using long-distance microscopy. We focus on two particularly relevant reference conditions where the ambient gas is $p_1 = 29\ bar, T_1 = 440\ K$ and $p_2 = 60\ bar$, $T_2 = 900\ K$. The goal was to maintain constant ambient density conditions at $\rho = 22.8\ kg/m^3$ while at the same time injecting the liquid at supercritical pressure in both cases. By preserving the ambient density, similar jet penetration and gas-liquid interaction forces are maintained and thus the effects of pressure, temperature, and the resultant multicomponent property variations on phase transitions are isolated.

Using the two reference conditions described above for n-dodecane, we repeated the LES analysis performed for the baseline n-heptane case and obtained trends similar to those shown in Fig. 5. We then directed our attention to the imaging experiments to gain further insights. Figure 6 compares the development of the liquid fuel structure at the two reference conditions. Sequences of images at the end of injection are shown when the velocity of the injected fuel approaches zero. This results in much less aerodynamic drag. Despite imperfect optical resolution, the low-temperature sequence clearly shows that individual ligaments still exist, which is evidence that surface tension forces still exist. Conversely, the high-temperature sequence appears to show a quite different process with no evidence of drops or ligaments. To explain this, we then developed a comprehensive theoretical model by combining the mixing line shown in Fig. 5 with VLE theory, which in turn provides the boundary conditions required for the LG model.

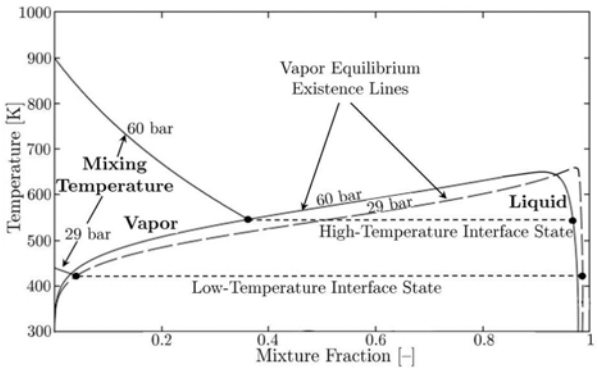

Figure 7: Mixing lines obtained from detailed analysis of the multicomponent mixture states (such as in Fig. 5) combined with VLE theory facilitate application of the LG model. The intersection of respective curves on the vapor side provide the baseline boundary conditions required to reconstruct the multicomponent interfaces.

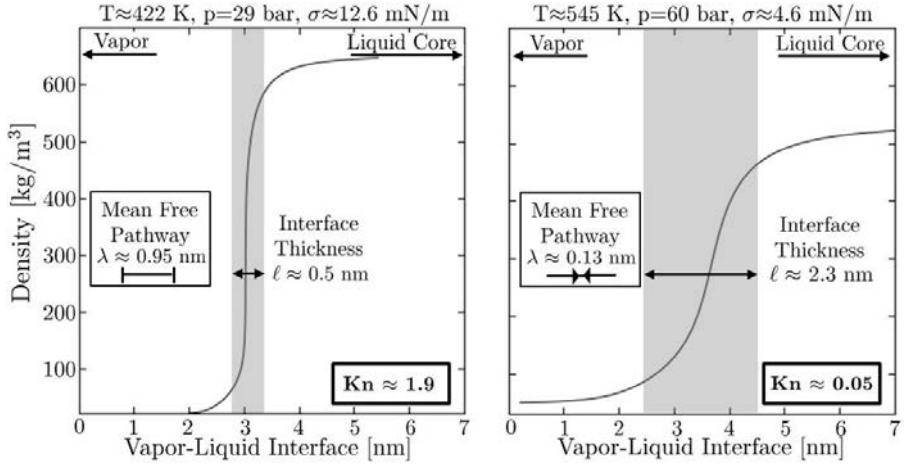

Figure 8: Detailed interface structure obtained using the integrated real-fluid, VLE and LG model provides insights with respect to the interfacial surface tension and thickness for the two n-dodecane reference cases. The high-temperature interface shows a substantially reduced surface tension and a wider interface thickness compared to the low-temperature interface. An applied Knudsen-number criterion further reveals continuous interfacial diffusion layers develop not necessarily because of vanishing surface tension forces, but also because of broadening vapor-liquid interfaces. The broadening interfaces, coupled with the fact that the mean free molecular path decreases significantly with pressure, shifts the interfacial structure from the molecular to continuum length scale regime.

Figure 7 shows the integrated combination of mixing lines for the two reference conditions combined with those from VLE theory. The intersection of the curves on the vapor side provide the boundary conditions that the LG model uses to reconstruct the interfaces. This intersection sets the thermophysical state of the mixture on either side of an assumed constant temperature gas-liquid interface. Using the VLE data as input for the LG model, we calculated the detailed interfacial structure of the two n-dodecane reference conditions. Results are summarized in Fig. 8. Analysis of these plots provides several revealing insights. First, the high-temperature interface exhibits not only a substantially reduced surface tension, but also a wider interface thickness compared to the low-temperature interface. An applied Knudsen-number criterion then further reveals that continuous interfacial diffusion layers develop not necessarily because of vanishing surface tension forces, but also because of the broadening vapor-liquid interfaces. The broadening interfaces, coupled with the fact that the mean free molecular path decreases significantly with pressure, effectively shifts the interfacial structure from the molecular to continuum length scale regime. Independent of any residual surface tension forces, the Navier-Stokes equations apply across these interfaces. Continuum based diffusion laws also apply, which produce a continuous phase transition within. These data provide an interestingly striking set of quantitative insights regarding liquid injection in high-pressure systems and the transitional phenomena that occur.

Summary and Conclusions

Past works have suggested that two extremes exist with regard to liquid injection in high-pressure systems. At lower pressures, the classical situation exists where a well defined interface separates the injected liquid from ambient gases due to the presence of surface tension. Under these conditions, surface tension forces form a discontinuous non-continuum interface that promotes primary atomization, secondary breakup, and the resultant spray phenomena that has been the well recognized and widely assumed. At high-pressure conditions, however, the situation can become quite different. Under these conditions, a distinct gas-liquid interface may not exist. Effects of surface tension become diminished and the lack of these inter-molecular forces minimizes or eliminates the formation of drops and promote diffusion dominated mixing processes prior to atomization. In this paper, we have presented some of the first evidence that diffusion dominated mixing, not atomization, occurs at certain Diesel engine conditions. In addition, we have presented a theoretical analysis that explains why and quantifies the change in the interfacial dynamics that leads to the transition between the classical non-continuum "jump" conditions associated with two-phase flows and the continuous gas-liquid interfacial diffusion layers.

To frame the observations described above, we performed both LES to understanding aspects related to the state of the local mixture and have corroborated our findings through experimental observations. Experimental imaging of injection processes suggests that drop formation occurs at low ambient temperature, but diffusion dominated mixing occurs without apparent formation of fuel drops at engine-relevant high ambient temperature conditions. To explain this transition, we extended our real-fluid model to account for multicomponent vapor-liquid equilibrium, the presence of surface tension, and the interface states for two investigated chamber conditions. Using this framework, linear gradient theory was then applied to reconstruct the detailed interface structure. The high-temperature interface showed a substantially reduced surface tension and a wider interface thickness compared to the low-temperature interface. An applied Knudsen-number criterion then revealed a major finding. Contrary to conventional wisdom, gas-liquid interfacial diffusion layers develop not necessarily because of vanishing surface tension forces, but because of broadening vapor-liquid interfaces. These interfaces become so thick that they enter the continuum length scale regime. Thus, independent of any residual surface tension forces that might be present, the Navier-Stokes equations apply across the high-temperature vapor-liquid interface if the viscous stress term is modified appropriately. Similarly, continuum based diffusion laws apply across the vapor-liquid interface, producing a continuous phase transition. Similar conditions are anticipated for more complex and realistic multicomponent Diesel fuels since their critical properties are comparable to those of n-dodecane. Future work will build on these observations to develop a clear understanding of the transitional nature of interfacial multiphase flow dynamics as a function of pressure.

Acknowledgements

Support for this research was provided jointly by the U.S. Department of Energy, Office of Energy Efficiency and Renewable Energy, Vehicle Technologies Program and the Office of Science, Basic Energy Sciences Program. The research was performed at the Combustion Research Facility, Sandia National Laboratories, Livermore, California. Sandia is a multiprogram laboratory operated by the Sandia Corporation, a Lockheed Martin Company, for the United States Department of Energy's National Nuclear Security Administration under contract DE-AC-94AL85000.

References

[1] M. Oschwald, J. Smith, R. Branam, J. Hussong, A. Schik, B. Chehroudi, and D. Talley. Injection of fluids into supercritical environments. *Combustion Science and Technology*, 178(1-3):49–100, 2006.

[2] M. Habiballah, M. Orain, F. Grisch, L. Vingert, and P. Gicquel. Experimental studies of high-pressure cryogenic flames on the mascotte facility. *Combustion Science and Technology*, 178(1-3):101–128, 2006.

[3] K.-C. Lin, S. Cox-Stouffer, and T. Jackson. Structures and phase transition processes of supercritical methane/ethylene mixtures injected into a subcritical environment. *Combustion Science and Technology*, 178(1-3):129–160, 2006.

[4] S. Candel, M. Juniper, G. Singla, P. Scouflaire, and C. Rolon. Structure and dynamics of cryogenic flames at supercritical pressure. *Combustion Science and Technology*, 178(1-3):161–192, 2006.

[5] N. Zong and V. Yang. Cryogenic fluid jets and mixing layers in transcritical and supercritcal environments. *Combustion Science and Technology*, 178(1-3):193–228, 2006.

[6] J. C. Oefelein. Mixing and combustion of cryogenic oxygen-hydrogen shear-coaxial jet flames at supercritical pressure. *Combustion Science and Technology*, 178(1-3):229–252, 2006.

[7] J. Bellan. Theory, modeling and analysis of turbulent supercritical mixing. *Combustion Science and Technology*, 178(1-3):253–281, 2006.

[8] L. C. Selle, N. A. Okong'o, J. Bellan, and K. G. Harstad. Modelling of subgrid-scale phenomena in supercritical transitional mixing layers: An a priori study. *Journal of Fluid Mechanics*, 593:57–91, 2007.

[9] G. Ribert, N. Zong, V. Yang, L. Pons, N. Darabiha, and S. Candel. Counterflow diffusion flames of general fluids: Oxygen/hydrogen mixtures. *Combustion and Flame*, 154:319–330, 2008.

[10] G. Lacaze, B. Cuenot, T. Poinsot, and M. Oschwald. Large eddy simulation of laser ignition and compressible reacting flow in a rocket-like configuration. *Combustion and Flame*, 156:1166–1180, 2009.

[11] L. Pons, N. Darabiha, S. Candel, G. Ribert, and V. Yang. Mass transfer and combustion in transcritical non-premixed counterflows. *Combustion Theory and Modelling*, 13:57–81, 2009.

[12] T. Schmitt, Y. Méry, M. Boileau, and S. Candel. Large-eddy simulation of oxygen/methane flames under transcritical conditions. *Proceedings of the Combustion Institute*, 33:1383–1390, 2011.

[13] L. M. Pickett. Engine combustion network. www.ca.sandia.gov/ECN, 2005-2012. Combustion Research Facility, Sandia National Laboratories.

[14] J. C. Oefelein. Large eddy simulation of turbulent combustion processes in propulsion and power systems. *Progress in Aerospace Sciences*, 42(1):2–37, 2006.

[15] J. C. Oefelein. Thermophysical characteristics of LOX–H_2 flames at supercritical pressure. *Proceedings of the Combustion Institute*, 30: 2929–2937, 2005.

[16] J. C. Oefelein, R. W. Schefer, and R. W. Barlow. Toward validation of LES for turbulent combustion. *AIAA Journal*, 44(3):418–433, 2006.

[17] J. C. Oefelein, V. Sankaran, and T. G. Drozda. Large eddy simulation of swirling particle-laden flow in a model axisymmetric combustor. *Proceedings of the Combustion Institute*, 31:2291–2299, 2007.

[18] J. H. Frank, S. A. Kaiser, and J. C. Oefelein. Analysis of scalar mixing dynamics in LES using high-resolution imaging of laser Rayleigh scattering in turbulent non-reacting jets and non-premixed jet flames. *Proceedings of the Combustion Institute*, 33:1373–1381, 2011.

[19] A. M. Kempf, B. J. Geurts, and J. C. Oefelein. Error analysis of large eddy simulation of the turbulent non-premixed Sydney bluff-body flame. *Combustion and Flame*, 158:2408–2419, 2011. doi: 10.1016/j.combustflame.2011.04.012.

[20] J. C. Oefelein, R. N. Dahms, and G. Lacaze. Detailed modeling and simulation of high-pressure fuel injection processes in diesel engines. *SAE International Journal of Engines*, 5(3):1–10, 2012. doi: 10.4271/2012-10-1258.

[21] T. W. Leland and P. S. Chappelear. The corresponding states principle. A review of current theory and practice. *Industrial and Engineering Chemistry Fundamentals*, 60(7):15–43, 1968.

[22] J. S. Rowlinson and I. D. Watson. The prediction of the thermodynamic properties of fluids and fluid mixtures–I. The principle of corresponding states and its extensions. *Chemical Engineering Science*, 24(8):1565–1574, 1969.

[23] R. C. Reid, J. M. Prausnitz, and B. E. Polling. *The Properties of Liquids and Gases*. McGraw-Hill, New York, New York, 4th edition, 1987.

[24] G. J. VanWylen and R. E. Sonntag. *Fundamentals of Classical Thermodynamics*. John Wiley and Sons, Incorporated, New York, New York, 3rd edition, 1986.

[25] S. Gordon and B. J. McBride. Computer program for calculation of complex chemical equilibrium compositions, rocket performance, incident and reflected shocks and Chapman-Jouguet detonations. Technical Report NASA SP-273, National Aeronautics and Space Administration, 1971.

[26] R. J. Kee, F. M. Rupley, and J. A. Miller. Chemkin thermodynamic data base. Technical Report SAND87-8215B, Sandia National Laboratories, 1990. Supersedes SAND87-8215 dated April 1987.

[27] J. F. Ely and H. J. M. Hanley. Prediction of transport properties. 1. Viscosity of fluids and mixtures. *Industrial and Engineering Chemistry Fundamentals*, 20(4):323–332, 1981.

[28] J. F. Ely and H. J. M. Hanley. Prediction of transport properties. 2. Thermal conductivity of pure fluids and mixtures. *Industrial and Engineering Chemistry Fundamentals*, 22(1):90–97, 1981.

[29] R. B. Bird, W. E. Stewart, and E. N. Lightfoot. *Transport Phenomena*. John Wiley and Sons, Incorporated, New York, New York, 1960.

[30] J. O. Hirschfelder, C. F. Curtiss, and R. B. Bird. *Molecular Theory of Gases and Liquids*. John Wiley and Sons, Incorporated, New York, New York, 2nd edition, 1964.

[31] S. Takahashi. Preparation of a generalized chart for the diffusion coefficients of gases at high pressures. *Journal of Chemical Engineering of Japan*, 7(6):417–420, 1974.

[32] J. W. Cahn and J. E. Hilliard. Free energy of a nonuniform system. I. Interfacial free energy. *Journal of Chemical Physics*, 28(2):258–267, 1958.

[33] E. A. Müller and A. Mejía. Interfacial properties of selected binary mixtures containing n-alkanes. *Fluid Phase Equilibria*, 282:68–81, 2009. doi: 10.1016/j.fluid.2009.04.022.

[34] A. Mejía, J. C. Pàmies, D. Duque, H. Segura, and L. F. Vega. Phase and interfacial behaviors in type-I and type-V Lennard-Jones mixtures: Theory and simulations. *Journal of Chemical Physics*, 123(034505):1–10, 2005. doi: 10.1063/1.1955529.

[35] C. Miqueu, J. M. Míguez, M. M. Pi neiro, T. Lafitte, and B. Mendiboure. Simultaneous application of the gradient theory and monte carlo molecular simulation for the investigation of methane/water interfacial properties. *Journal of Physical Chemistry B*, 115:9618–9625, 2011. doi: 10.1021/jp202276k.

[36] J. C. Oefelein and G. Lacaze. Low-temperature injection dynamics and turbulent flame structure in high-pressure supercritical flows. *Proceedings of the 23rd International Colloquium on the Dynamics of Explosions and Reactive Systems*, July 24-29 2011. Irvine, California.

[37] R. N. Dahms, L. M. Pickett, and J. C. Oefelein. A dense fluid approximation for the simulation of Diesel engine fuel injection processes. *Proceedings of the 23rd Annual Conference on Liquid Atomization and Spray Systems*, May 15-18 2011. Ventura, California.